J MATER SCI 41 (2006) 927–936

Effect of acrylic copolymer and terpolymer composition on the properties of *in-situ* polymer/silica hybrid nanocomposites

S. PATEL, A. BANDYOPADHYAY*, V. VIJAYABASKAR, ANIL K. BHOWMICK†
Rubber Technology Centre, Indian Institute of Technology, Kharagpur-721302, India
E-mail: anilkb@rtc.iitkgp.ernet.in

Acrylic copolymer- and 5% acrylic acid (AA) modified terpolymer-silica hybrid nanocomposites were synthesized by free radical bulk polymerization of ethyl acrylate (EA), butyl acrylate (BA) and acrylic acid (AA) with simultaneous generation of silica from tetraethoxysilane by sol-gel reaction. The pure polymers were analyzed by using Fourier Transform infrared (FTIR) spectroscopy and solid state nuclear magnetic resonance (NMR) spectroscopy. The hybrid samples were characterized by scanning electron microscopy (SEM), FTIR spectroscopy, NMR spectroscopy, dynamic mechanical, mechanical and thermal properties. SEM images confirmed the presence of nanosilica particles within the polymer matrices, whose dispersion and particle size distribution and visual appearance were dependent on the relative polarity (hydrophilicity) of the polymer matrices and the concentration of the filler. There was no evidence of strong chemical interaction between the polymers and the dispersed silica phase, as confirmed from the FTIR results. Terpolymer-silica hybrids demonstrated superior mechanical properties compared to the copolymer-silica hybrids. They also showed higher dynamic storage modulus and positive shift in the loss tangent peaks. The thermal stability of the nanocomposites was marginally higher which was possibly due to the dipolar interaction at the organic-inorganic interface.

1. Introduction

In recent years, great attention has been paid to polymer-inorganic hybrid nanocomposites. This is mainly due to exciting physical [1], optical [2], chemical [3], flame retardancy [4], electrical [5], gas permeability [6] and magnetic [7] properties, which are superior to those of conventional polymer composites. Organic–inorganic hybrid nanocomposites demonstrate an effective combination of properties of the organic polymers (flexibility, low density etc) and the inorganic inclusions (rigidity, hardness, thermal stability etc). Clay (one dimensional) and silica (zero dimensional) are most popularly used as the inorganic nanofiller within a nanocomposite. From our laboratory, a number of research papers has been published so far on clay and silica nanocomposites based on various rubbers [8–13]. Since the properties of these materials are directly related to the morphology of the systems, the dispersion of the inorganic phase plays an important role in connection with the above mentioned properties. Poor interaction between the organic and the inorganic components results in poor dispersion of the nanofiller, which ultimately leads to inferior properties. In contrast, strong interactions and finer dispersion of the same display unique properties not shared by their microcounterparts or conventionally filled polymers. The major problem, which arises during synthesis of high performance homogeneous hybrid composites, especially with silica, is how to control the phase separation between inorganic and organic components. Recently, few researchers utilized polymers functionalized with trialkoxysilane moieties to facilitate crosslinking reaction with inorganic fillers like silica and successfully retarded the phase separation [14–18]. Alternatively, judicious selection of polymer structures can make systems more compatible with the inorganic phase

Present Address: Department of Polymer Science & Technology, University of Calcutta, 92, A.P.C. Road, Calcutta-700009, India.
†Author to whom all correspondence should be addressed.
0022-2461
DOI: 10.1007/s10853-006-6576-x

and hence can help in increasing interfacial interaction via hydrogen bonds, covalent bond, van der Waals or dipolar interaction [19].

In-situ polymerization for synthesizing organic-inorganic hybrid composites is an interesting approach as the high performance polymer nanocomposites with silica as nano-dispersed phase could be produced by this technique [20–24]. Till now optically transparent and homogeneous *in-situ* polymer-silica hybrid nanocomposites have been reported using poly(methyl methacrylate) [20], poly(2-hydroxyethyl acrylate) [21], poly(hydroxyl methylacrylate) [22] and polystyrene[23] by *in-situ* polymerization simultaneously with sol-gel reaction of Tetraethoxysilane (TEOS used as silica precursor). The concurrent formation of the two phases can result in a highly homogeneous type of materials even with the high silica concentration. The kinetics of sol-gel synthesis can be controlled by judicious selection of reaction conditions like catalyst type and concentration, pH, H_2O: Si mole ratio, initiator concentration, solvent and temperature and hence influence final properties of nanocomposites. Simultaneous and rapid kinetics of the two reactions-hydrolysis and condensation may avoid phase separation and produce homogeneous materials. The interactions between the polar organic monomers and the surface hydroxyl groups of the sol-gel products through hydrogen bonding, dipole interaction etc. can help in preventing macrophase separation [24]. But till date, there is no published report on the effect of microstructure i.e. copolymer and terpolymer compositions on the synthesis and properties of *in-situ* polymer-silica hybrids. Therefore, the objective of the present work is to study the effects of acrylic copolymer/terpolymer composition and interaction between the polymer and the nanofiller on the synthesis and properties of *in-situ* polymer-silica hybrids by sol-gel technique. Rubbery acrylic copolymer/terpolymer -silica nanocomposites have been synthesized by free radical bulk polymerization of ethyl acrylate (EA), butyl acrylate (BA), and acrylic acid (AA) with simultaneous generation of *in-situ* silica by sol-gel reaction.

2. Experimental

2.1. Materials

Tetraethoxysilane (TEOS, density = 930 kg/m^3, boiling point 168°C) was procured from Acros Organics, Pittsburgh (USA). Ethyl acrylate (EA) was supplied by Burgoyne Burbidges & Co, Mumbai (India). Butyl acrylate (BA) and acrylic acid (AA) were procured from Loba Chemie Pvt. Ltd., Mumbai (India). Benzoyl peroxide (BPO, 97% purity) was purchased from Aldrich Chemicals, Milwaukee (USA). Hexamethylethelenediamine carbamate (HMDC, DIAK#1) was generously supplied by NICCO Corp. Ltd., Shyamnagar (India). Tetrahydrofuran (THF, 99% pure) was procured from Merck Ltd., Mumbai (India). Sodium hydroxide, deionized water and formic acid, all of laboratory grade, were obtained from indigenous sources.

2.2. Preparation of hybrid composites

EA and BA were purified by repeated washing with 4% aqueous NaOH solution followed by vacuum distillation. AA was purified by vacuum distillation only. *In-situ* polymer-silica hybrids were synthesized by free radical bulk polymerization of monomers and simultaneous *in-situ* silica generation by the sol-gel reaction. All the reactants (purified 30 gm of monomers, BPO as initiator (0.06 wt% of monomer), formic acid, TEOS and H_2O in 1:2 molar proportions) were taken in the reactor. The pH of the medium was adjusted at 1–2 by addition of appropriate amount of formic acid. The polymerization and sol-gel reactions were carried out under inert nitrogen atmosphere at 80°C for 30 min. The TEOS concentration was varied from 10 to 50 wt% with respect to the monomers. Polymerization conditions like time, temperature, pH etc. were optimized by calculating percentage conversion and gel contents. The entire reaction was deliberately stopped at a lower conversion (50–60%) to prevent gelation. The relative kinetics of simultaneous polymerization and sol-gel synthesis were studied by varying concentration of sol-gel catalyst and reaction temperatures (60, 65, 70 and 80°C). In order to prepare cured hybrid composites, HMDC was mixed with the uncured hybrid samples on a two roll mill followed by compression moulding. Curing of the moulded thin sheet was done in an air oven at 170°C for 30 min followed by 24 h post curing at 70°C. Curing conditions were optimized by measuring the gel content of the resultant samples. The details of sample compositions used in this study are listed in Table I.

3. Characterization of the pure polymer and the hybrid composites

3.1. Infrared (IR) spectroscopy

The infrared (IR) spectroscopic study was carried out to characterize both the neat polymer and the hybrid composite films. All the spectra were recorded with a Nicolet Nexus Fourier Transform Infrared spectrometer (FTIR) in ATR (attenuated total internal reflection) mode by using 45 ° KRS5 prism at room temperature. The samples were scanned from 4000 to 600 cm^{-1} with a resolution of 4 cm^{-1}. All the spectra were taken after an average of 32 scans for each specimen.

3.2. Solid state nuclear magnetic resonance (NMR) spectroscopy

The solid state C-13 Fourier Tansform nuclear magnetic resonance (FTNMR) experiments were performed

TABLE I Compositions of the hybrid composites

Sample designation	Theoretical EA (wt%)	Theoretical BA (wt%)	Theoretical AA (wt%)	TEOS (wt%) of polymer	HMDC (wt%) of polymer	Appearance of the films
85_E	85	15	—-	—	—	Transparent
85_EN_{10}	85	15	—-	10	—	Transparent
$8E_5N_{20}$	85	15	—-	20	—	Transparent
85_EN_{30}	85	15	—-	30	—	Transparent
85_EN_{40}	85	15	—-	40	—	Transparent
85_EN_{50}	85	15	—-	50	—	Transparent
5_A85_E	85	15	5	—	—	Transparent
$5_A85_EN_{10}$	85	15	5	10	—	Transparent
$5_A85_EN_{20}$	85	15	5	20	—	Transparent
$5_A85_EN_{30}$	85	15	5	30	—	Transparent
$5_A85_EN_{40}$	85	15	5	40	—	Transparent
$5_A85_EN_{50}$	85	15	5	50	—	Transparent
85_EX	85	15	—-	—	2.5	Translucent
$85_EN_{30}X$	85	15	—-	30	2.5	Translucent
$85_EN_{50}X$	85	15	—-	50	2.5	Translucent
5_A85_EX	85	15	5	—	2.5	Translucent
$5_A85_EN_{30}X$	85	15	5	30	2.5	Translucent
$5_A85_EN_{50}X$	85	15	5	50	2.5	Translucent

at 75.5 MHz on a Bruker 300 MSL spectrometer. Magic angle spinning (MAS) and high power proton decoupling were used with cross polarization (CP) to obtain the spectra. The spinning speeds ranged from 1.0 to 3.0 kHz at 70°C. The spectral width was 29240 Hz and 512 data points with acquisition time of 0.014 second were collected for each spectrum.

3.3. Scanning electron microscopy (SEM) and energy dispersive X-ray (EDX) silicon mapping

Dispersion of silica particles in the polymer matrices was observed through microscopic investigations with a JEOL JSM 5800 scanning electron microscope. The samples were sputter coated with gold in order to avoid the artifacts associated with sample charging. All the images were taken with an acceleration voltage of 20 kV. The statistical average of the diameters of the *in-situ* generated silica particles was calculated by randomly choosing 50 particles (which included the smallest and the largest diameter particles) from each sample. The X-ray silicon mapping (EDX) of the hybrid composite films was recorded in an Oxford EDAX system, attached to the microscope.

3.4. Determination of mechanical properties

The mechanical properties of the crosslinked neat polymers and their hybrid composites were determined by a Universal Testing Machine (UTM, Zwick 1445) on tensile dumbbell specimens, punched out from the cast films by using ASTM Die C. The tests were carried out as per ASTM D 412–99 method at ambient temperature with a grip separation speed of 500 mm/min. The average value of three tests is reported for each sample.

3.5. Dynamic mechanical thermal analysis (DMTA)

Dynamic mechanical thermal characteristics of the hybrid composite films were evaluated in a DMTA IV (RHEOMETRIC SCIENTIFIC) under tension mode. The experiments were carried out at a frequency of 1 Hz in the temperature range of −60°C to 70°C at a heating rate of 2°C/min. The data were analyzed using RSI Orchestrator application software on an ACER computer attached to the machine. The storage modulus and loss tangent (tan δ) characteristics were measured for all the samples under identical conditions.

3.6. Thermogravimetric analysis (TGA)

Themogravimetric analysis of the crosslinked hybrid composites was performed by using a DuPont TGA instrument (Model no. 2000) from ambient temperature to 800°C at a programmed heating rate of 20°C/min in nitrogen atmosphere. A sample weight of ∼10 mg was taken for all the measurements. The weight loss against temperature was recorded.

4. Results and discussion

4.1. Infrared spectroscopic (FTIR) analysis

The FTIR spectra of the representative specimens i.e. pure acrylic copolymer and 5% AA modified terpolymer are shown in Fig. 1. The characteristic peaks are assigned in Table II [25]. The strong absorption bands in the range

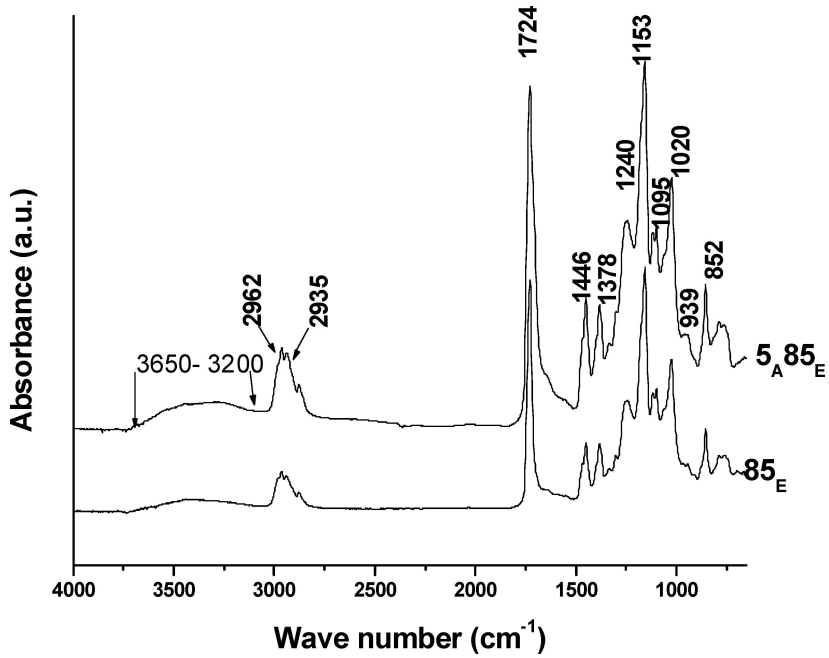

Figure 1 FTIR spectra of representative neat polymers.

of 1720–1730 cm^{-1} and at 1153 cm^{-1} corresponds to carbonyl (>C=O) and asymmetric C–O–C stretching vibrations present in both copolymer and 5% AA modified terpolymer samples. In the terpolymers, differentiation between ester >C=O and acid >C=O could not be made since both the peaks merge to exhibit a single band at 1724 cm^{-1}. Absorption band due to O-H stretching in the region of 3000–3200 cm^{-1} is due to some absorbed moisture in the sample. In the case of terpolymer samples, contribution from acid –COOH group is also probable from its higher intensity. Absorption bands at 1446, 1378 and 2960 cm^{-1} are due to C–H bending, C–H deformations of the alkyl part and C–H stretching vibration of $O–C_2H_5$ groups respectively. Absorption bands due to symmetric C–O–C and asymmetric C–O–C stretching vibrations of the acrylates appear at 1153 cm^{-1} and 1240 cm^{-1} respectively. The skeletal vibration of the acrylates is observed in the range of 1020–1095 cm^{-1} in both the copolymer and the terpolymer. An associated peak of C–O–C deformation of the acrylate is also present at 852 cm^{-1}.

The FTIR spectra of the representative uncured *in-situ* copolymer- and 5% AA modified terpolymer-silica hybrids prepared from 30 wt% initial TEOS concentration are shown in Fig. 2. The characteristic peaks are assigned in Table II. The peak position of 1724 cm^{-1} corresponding to C=O stretch remains almost unaffected in both the copolymer and the terpolymer hybrid composites. This indicates that these systems lack strong chemical interaction at the organic-inorganic interface. However, the presence of weak secondary interactions that could not be detected in the spectra, cannot be ruled out. This could be weak hydrogen bonding, polar-polar type or dipole induced –dipolar type of interactions. Absorption peak due to Si–O–Si stretching of silica appears in the region of 1000–1100 cm^{-1} and merges with that of the C–O–C asymmetric stretching vibrations of the acrylic polymers. The shoulder in the absorption peaks at 1090 cm^{-1} and 1020 cm^{-1} is probably due to different configurations (ring and chain type) of the silica phase within the hybrid composites. The higher absorption value (1090 cm^{-1}) is mainly for three and four membered siloxane ring and the lower absorption value (1020 cm^{-1}) is principally due to linear Si–O–Si configuration [26]. Appearance of small band at 939 cm^{-1} is due to Si-O stretch of silanol groups indicating the presence of some uncondensed silanol in these hybrid composites.

TABLE II FTIR peak assignments for pure polymers and their hybrid composites

Wave number (cm^{-1})	Functional group
3600–3200	–OH stretching
2960	Asymmetric –CH stretching
2935	–CH stretching
1724	>C=O stretching
1446	–C–H bending
1378	–C–H deformation
1240, 1153	Asymmetric C–O–C stretchings
1020, 1095	Skeletal vibration of acrylate, Si–O–Si stretching
939	Si–O stretch of silanol
852	C–O–C deformation

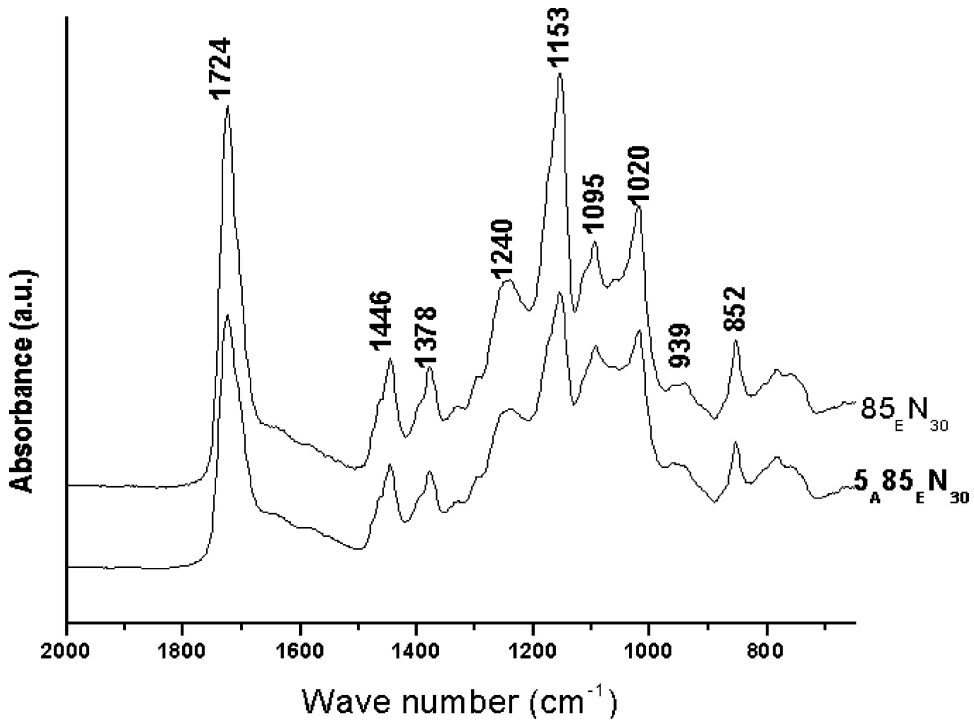

Figure 2 FTIR spectra of the representative hybrid composites.

4.2. Solid state nuclear magnetic resonance (NMR) spectroscopic analysis

The C-13 solid state NMR spectra for the pure terpolymer of EA, BA and AA in the ratio of 85:15:5 and its hybrid composites containing 30 wt% of TEOS were taken. The spectrum of the terpolymer recorded at 70°C is shown in Fig. 3. A similar spectrum was obtained for the hybrid composites. It is clear that the peaks are sharper for the sample and line broadening is avoided (Fig. 3). This indicates that ^{13}C spin relaxation times of those carbons in that ppm range are short at higher temperature and this condition is sufficient for accurate quantification of different peaks [27]. Characteristic peak corresponding to carboxylic group of acrylic acid is observed at 174 ppm in both terpolymer and its hybrid nanocomposites. It is difficult to distinguish between the ester and the carboxylic peaks. Peaks at 175.3 and 176.2 ppms are observed with low intensities for the ester groups of BA and EA respectively. Peaks corresponding to $–CH_3$ and $–CH_2$ groups of the ester present in BA are found at 14.4 and 19.5 ppm. Both the terpolymer and the silica hybrid nanocomposites have shown several peaks in the range of 20–60 ppm, which are due to the presence of the aliphatic groups. This will correspond to $–CH_2$- and –CH- linkages due to a particular sequence distribution. In the case of hybrid composites, peaks at 63.9 and 15.4 ppm of less intensity are observed due to the presence of ethoxy groups in silica network. This has also resulted in higher intensity peaks for $–CH_2$ and –CH groups in the polymer matrix, as indicated in the stacked spectra (Fig. 3b). An attempt has been made to study the sequence of the two monomers distributed in the polymer chain. This involves the assumption of various sequences such as HTHT, HHTT, HTTH, HHHH, TTTT, HTTT and HHHT respectively. The theoretical carbon resonance are calculated as per additivity principle and compared with the values in Sadtler guide [28]. Peaks at 26.2 and 33.1 ppms corresponding to $–CH_2$ groups and at 60.7and 43.3 ppm for –CH groups in HHTT structure are observed in both the cases. The neat terpolymer and its hybrid composites have an arrangement of poly(ethyl acrylate) in HHTT sequence separated by BA units. These imply that simultaneous synthesis of organic and inorganic phase has not affected the microstructure of the polymer. This indirectly also infers the absence of chemical interaction between the organic and the inorganic phase in the hybrid composites. A similar observation has been reported for the neat polymer in our earlier paper [27].

4.3. Microscopic observations

The SEM pictures of the representative *in-situ* polymer-silica hybrid composites (85_EN_{30}, $5_A85_EN_{30}$, $5_A85_EN_{50}$) are compared in Fig. 4a–c. Fig. 4a–b shows the morphology of the hybrid composites prepared from 30 wt% TEOS, while Fig. 4c displays the same at 50 wt% TEOS concentration. 85_EN_{30} hybrid composite shows spherical silica particles ranging in size from 50–250 nm with an average size of 85 nm (having standard deviation of 5.6) (Fig. 4(a). In contrast, the SEM micrograph of $5_A85_EN_{30}$

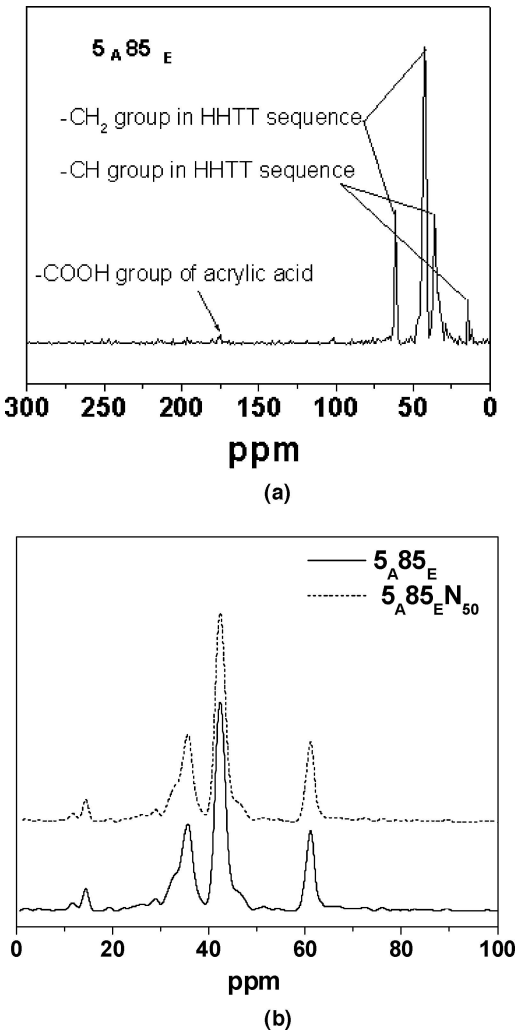

Figure 3 (a) NMR spectra of terpolymer 5_A85_E. (b) Stacked NMR spectra for 5_A85_E and $5_A85_EN_{50}$ in the region of 30–100 ppm.

in Fig. 4b registers somewhat reduced particles size distribution (30–175 nm) with an average diameter of 55 nm (having standard deviation of 8.0). $5_A85_EN_{30}$ shows better dispersion of silica compared to 85_EN_{30}. This discrimination is probably due to the increased polarity (hydrophilicity) of acrylate monomers, which prevents aggregation of finer silica particles by favorable interaction [29]. With increase in TEOS concentration from 30 to 50 wt%, the average silica particle size also increases. Fig. 4(c) shows average silica particles of 70 nm (having standard deviation of 5.0) in $5_A85_EN_{50}$ hybrid composite.

EDX study of the hybrid composites in Fig. 5a–c reflects the dispersion-aggregation phenomenon of silica within the polymer matrices. The white spots over the dark background indicate the location of silicon within the hybrid composites. Fig. 5(a)-(b) corresponds to hybrid composites 85_EN_{30} and $5_A85_EN_{30}$, which show almost uniform distribution of silicon. Slightly better dispersion of white spots in Fig. 5b compared to Fig. 5a indicates better dispersion of silica in $5_A85_0N_{30}$. On increasing TEOS concentration from 30 to 50 wt%, the white spots become denser which is due to more silica present in $5_A85_EN_{50}$. Owing to this uniform dispersion of nano silica particles, all the hybrid composites are optically transparent (Table I).

4.4. Mechanical properties

Tensile strength (and maximum tensile stress in the case of uncured samples), tensile modulus (@50% & 300%) and elongation at break values for all the uncrosslinked and crosslinked samples are recorded in Table IIIa–b. The tensile stress-strain plots of the representative uncured and cured hybrids are displayed in Fig. 6a–b. *In-situ* copolymer and terpolymer-silica hybrids show gradual increment in maximum tensile stress and modulus with increasing TEOS concentration. 350% increment in maximum tensile stress is obtained with $5_A85_EN_{50}$, while this is only 116% in the case of 85_EN_{50}. This is due to increased hydrophilicity of the monomer mixture, which may help in controlling the particle size of the *in-situ* generated silica during polymer synthesis. Increased hydrophilicity of the terpolymer also helps in uniform dispersion of the nanosilica as already discussed under the morphological analysis section. The same trend is recorded in the case of modulus at 50% elongation, which further indicates the higher extent of polymer-silica interaction within the hybrid composites on increasing polarity. Interestingly all the uncrosslinked terpolymer-silica hybrids do not show yielding due to the same above reason (Fig. 6(a)). The copolymer/silica hybrids in the uncured state register very high elongation (800%) (Table IIIa), while the elongation at break is improved with an increase in concentration of TEOS in the case of the terpolymer hybrids. This is possibly due to better dispersion of nano-silica particles in the highly polar polymer matrix in the later compared to the former. On crosslinking, the tensile strength and modulus dramatically increases in the terpolymer-silica hybrids than that of the copolymer-silica system (Table IIIb). The former records a maximum of 178 and 194% improvement in tensile strength over the control sample, whereas these are only 55 and 74% respectively in the case of the latter at 30 and 50 wt% TEOS concentrations. This is possibly due to the synergetic effects of better silica dispersion and their interaction with more polar acrylic terpolymer along with crosslinking of the matrix. The elongation at break value decreases with increasing TEOS concentration for all the crosslinked hybrid composites.

4.5. Dynamic Mechanical Thermal Analysis (DMTA)

Fig. 7a–b shows the temperature dependence of dynamic storage modulus (log scale) and tan delta for the representative crosslinked copolymer and terpolymer silica hybrid

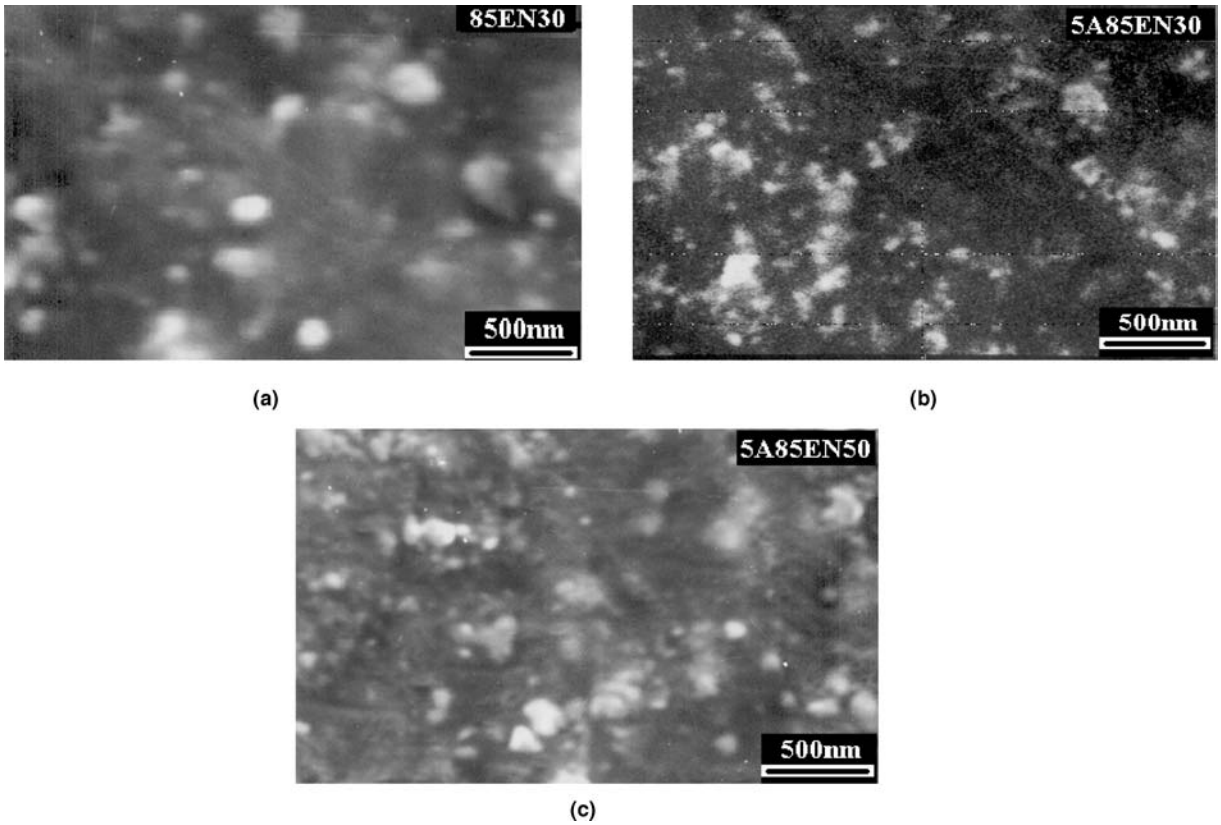

Figure 4 SEM micrographs of hybrid composites. (a) 85_EN_{30} (b), $5_A85_EN_{30}$, and (c) $5_A85_EN_{50}$.

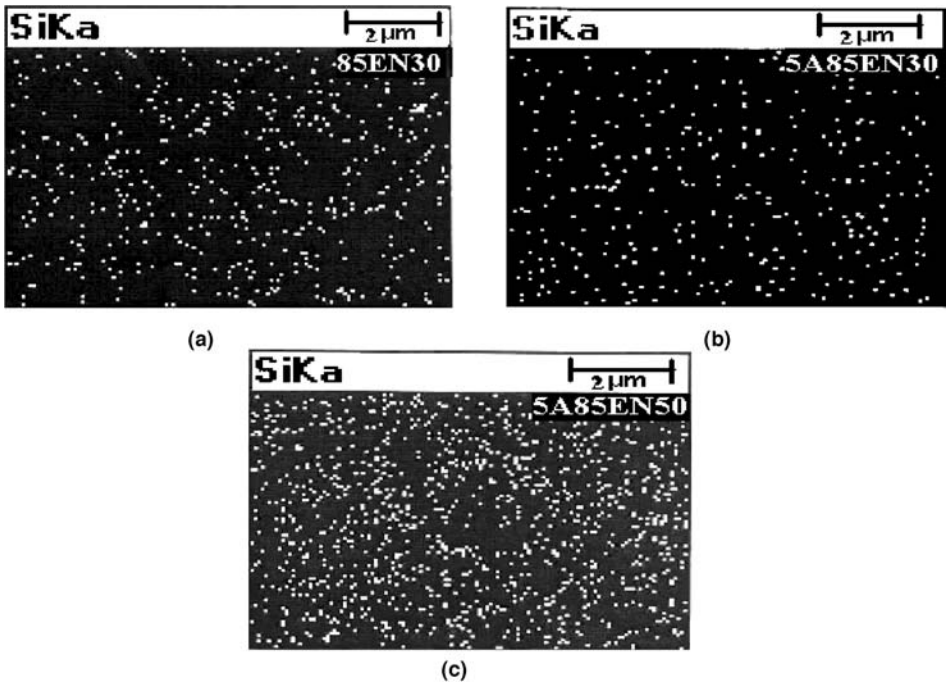

Figure 5 X-ray silicon mapping of hybrid composites. (a) 85_EN_{30}, (b) $5_A85_EN_{30}$, and (c) $5_A85_EN_{50}$.

nanocomposites. The results of the control sample are also included for the sake of comparison. The storage modulus vs temperature plots in Fig. 7a show sharp improvement in storage moduli for both the copolymer and the terpolymer nanocomposites over the entire temperature range, which results from reinforcing effect of the nanosilica. In the glassy region, 85_EN_{50} and $5_A85_EN_{50}$ nanocomposites register 55% and 105% increment in storage moduli over

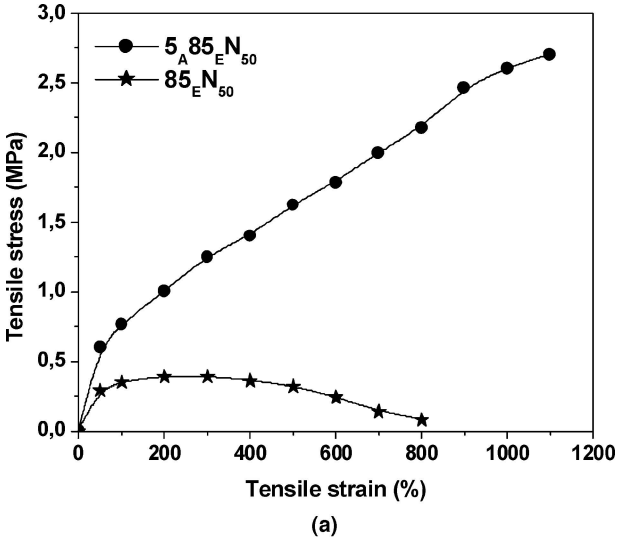

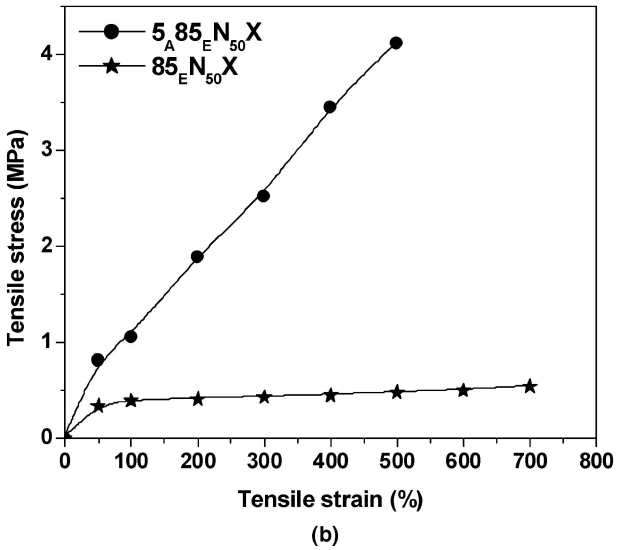

Figure 6 (a) Effect of polymer microstructure on the stress-strain properties of the uncured hybrid composites. (b) Effect of polymer microstructure on stress-strain properties of the cured hybrid composites.

their respective control samples. The effect of nanosilica reinforcement is more clearly visible in the rubbery region when the polymer matrix becomes soft. At room temperature, the copolymer hybrid with 50 wt% TEOS shows 157% increment in storage moduli, while in the case of the terpolymer hybrid with similar TEOS concentration, 177% increment is observed. This can be justified by the effect of increased hydrophilicity of the terpolymer matrix, which establishes favorable interfacial interaction with nanosilica, as already mentioned.

Remarkable changes in the viscous loss characteristics of the *in-situ* hybrid nanocomposites are visible from the tan δ vs temperature plots in Fig. 7b. All the samples exhibit a principal relaxation peak, corresponding to glass transition temperature. Both the copolymer and the 5% AA modified terpolymer nanocomposites show considerable reduction in the height of tanδ peak with

TABLE III (a) Mechanical properties of the uncured samples

Sample designation	Max. strength (MPa)	Modulus at 50% (MPa)	Elongation at break (%)
85_E	0.18	0.13	>800[a]
85_EN_{10}	0.25	0.17	>800[a]
$85E_{N20}$	0.29	0.19	>800[a]
85_EN_{30}	0.31	0.23	>800[a]
85_EN_{40}	0.33	0.25	>800[a]
85_EN_{50}	0.39	0.29	>800[a]
5_A85_E	0.56	0.31	>800[a]
$5_A85_EN_{10}$	1.46	0.39	492
$5_A85_EN_{20}$	1.73	0.42	805
$5_A85_EN_{30}$	1.90	0.46	800
$5_A85_EN_{40}$	2.40	0.50	1000
$5_A85_EN_{50}$	2.57	0.60	1100

[a]Indicates yielding after maximum stress, so the tests were aborted at 800% elongation.

TABLE III (b) Mechanical properties of the cured samples

Sample designation	Tensile strength (MPa)	Modulus at 50% (MPa)	Modulus at 300% (MPa)	Elongation at break (%)
85_EX	0.31	0.21	0.27	800
$85_EN_{30}X$	0.48	0.28	0.38	756
$85_EN_{50}X$	0.54	0.34	0.43	705
5_A85_EX	1.40	0.28	0.68	800
$5_A85_EN_{30}$ X	3.05	0.48	1.90	515
$5_A85_EN_{50}X$	4.11	0.81	2.52	497

respect to their control samples, indicating a decrease in viscous response of the samples within this temperature range. The nanocomposite, 85_EN_{50} registers 40% decrease in tanδ_{max}, whereas this decrease is 45% for $5_A85_EN_{50}$. The glass transition temperature corresponding to 85_E is $-27°C$, which is shifted to $-19°C$ in the case of 85_EN_{50}. On increasing hydrophilicity of 85_E by introducing AA, the terpolymer exhibits higher value of T_g with slightly decreased tanδ_{max} compared to 85_E, which is due to increased inter-chain interaction in the former. Also, the terpolymer nanocomposites show slightly greater shift in T_g (10°C) with much broader tanδ peak compared to the copolymer hybrids (8°C shift in Tg). These results are due to greater polymer-nanosilica interaction in the terpolymer hybrids than the copolymer-silica hybrids on account of increased polarity of the former. Decrease in tanδ_{max} height as well as broadening of tanδ peak with positive shift in T_g is a direct consequence of nanosilica interaction with polymer matrix, which leads to suppression of the mobility of polymer chains.

4.6. Themogravimetric analysis

Fig. 8 displays the TGA and DTG thermograms of representative crosslinked terpolymer-silica hybrid nanocom-

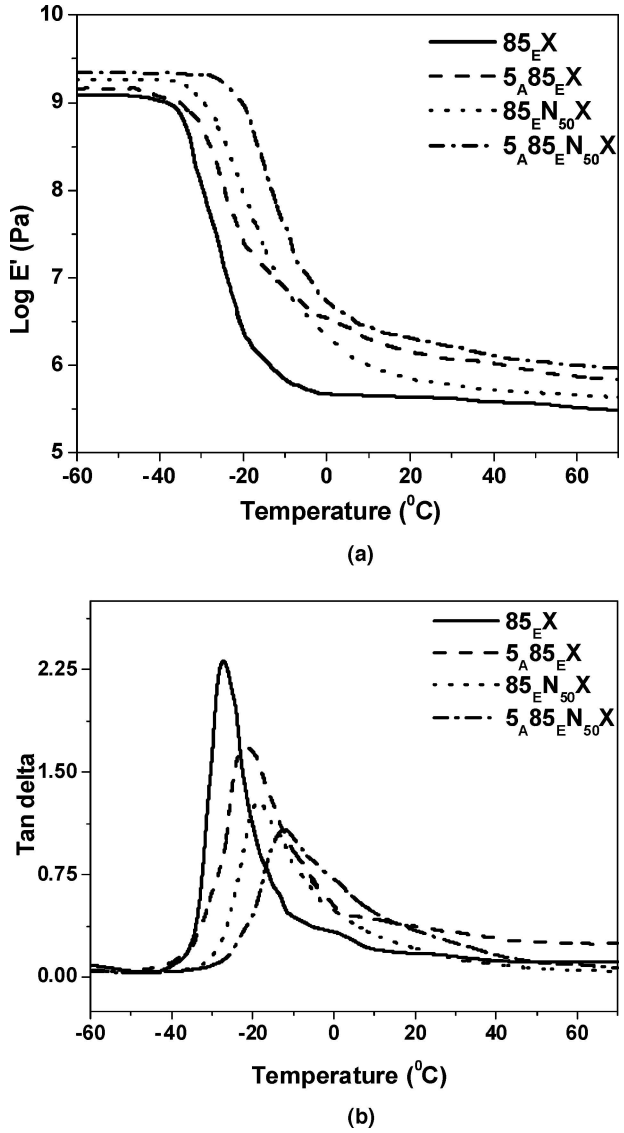

Figure 7 (a) Storage modulus versus temperature plots for the representative cured hybrids composites. (b) Tanδ versus temperature plots for the representative cured hybrids composites.

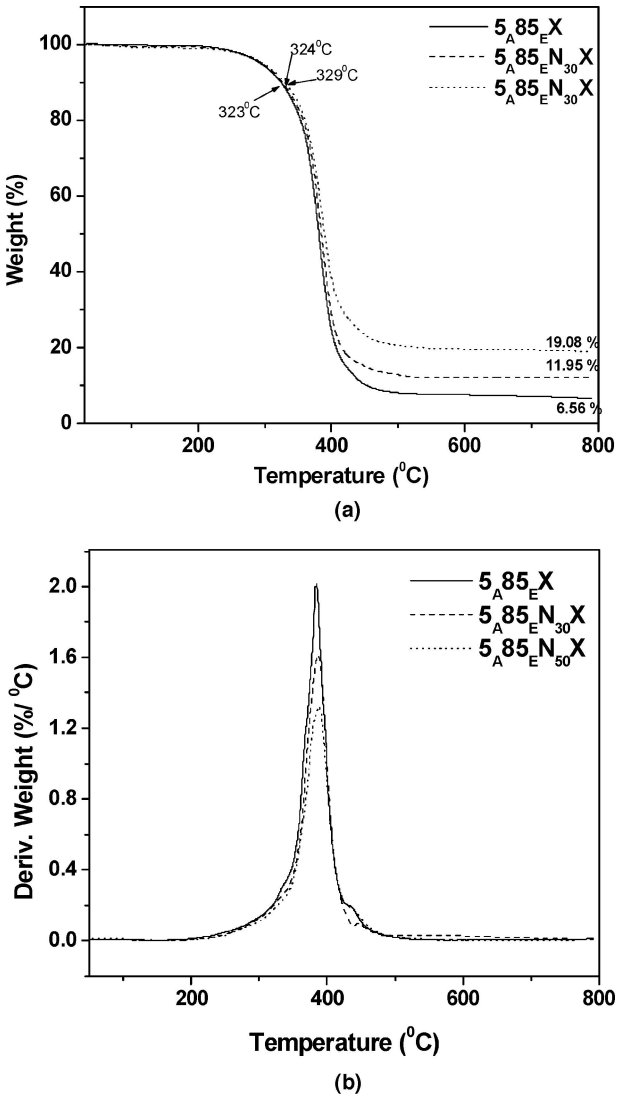

Figure 8 (a) TGA thermograms of the crosslinked control and the representative hybrid composites. (b) DTG thermograms of the crosslinked control and the representative hybrid composites.

posites. The decomposition temperature corresponding to initial 10% weight loss is shifted from 323°C in the pure 5_A85_E to 324°C in $5_A85_EN_{30}$ and 329°C in $5_A85_EN_{50}$. Marginal improvement in the onset of degradation temperature for *in-situ* terpolymer-silica hybrids is due to lack of any chemical interaction between the organic and the inorganic phase. This observation is also confirmed from the FTIR analysis where no shift in absorption peak due to >C=O stretching was observed for the silica hybrids. In contrast the lowering in the peak height of DTG plots in Fig. 8b is a clear evidence of reduced degradation rate of the hybrid composites. $5_A85_EN_{30}$ shows 20% decrease in the rate of thermal degradation at $T_{max.}$ On increasing the TEOS concentration from 30 to 50 wt%, the rate of degradation is further reduced by 35%. This is due to the presence of nanosilica in the matrix, imparting higher thermal stability to the hybrid composites. The residue obtained from these samples is black in color, indicating the char formation at the end of thermal degradation.

5. Conclusions

1. The *in-situ* acrylic copolymer- and the terpolymer-silica hybrid nanocomposites have been successfully synthesized by using ethyl acrylate, butyl acrylate and acrylic acid as the monomers and tetraethoxysilane as the silica precursor by the sol-gel technique. All the hybrid composites in the uncured state are visually transparent, while their crosslinked compositions are translucent. The transparent appearance of the composites ensures nanolevel

dispersion of the silica particles, which do not scatter light.

2. The SEM images of the uncrosslinked hybrid composites illustrate the presence of silica nanoparticles (average diameter <100 nm). it has been observed that the extent of polarity (and hydrophilicity) of the polymer backbone (acrylic co-/ter-polymer) controls the *in-situ* generated silica particle size. With high polarity, the average diameter of the silica particles is low. The sem results corroborate well with the EDX findings. In all the cases, no strong chemical interaction has occurred at the interfaces between the polymers and silica, as depicted from the FTIR and NMR analysis. The interaction is dipolar type, which increases with the introduction of acrylic acid.

3. AA modified uncrosslinked polymer/silica hybrid nanocomposites show higher improvement in maximum stress (356%) than the less polar copolymer hybrid composites (116%). A similar trend is also followed for the crosslinked samples. Significant increase in tensile modulus in the case of terpolymer-silica hybrids (190% as compared to only 74%) is due to the effect of higher polymer - silica interfacial interaction.

4. Strong increment in dynamic storage modulus indicates improved elastic response of the nanocomposites by more polymer adsorption over the silica particles. Positive shift of T_g and reduction in $\tan\delta_{max}$ value as well as broadening of $\tan\delta_{max}$ indicate decreased viscous characteristic of the nanocomposites.

5. The hybrid nanocomposites are thermally more stable than the control samples. The onset temperature is not improved drastically and this could be due to the lack of any chemical interaction at the organic-inorganic interfaces.

References

1. A. OKADA and A. USUKI, *Mater. Sci. Eng.* **3** (1995) 109.
2. A. BANDYOPADHYAY, A. K. BHOWMICK and M. D. SARKAR, *J. Appl. Polym. Sci.* **93** (2004) 2579.
3. P. JEDRZEJOWSKI, J. E. KLEMBERG-SAPIEHA and L. MARTINU, *Surf. Coati. Tech.* **188–189** (2004) 371.
4. J. W. GILMAN, *Appl. Clay Sci.* **15** (1999) 31.
5. P. B. MESSERSMITH and E. P. GIANNELIS, *J. Polym. Sci. Part A: Polym. Chem.* **33** (1995) 1047.
6. W. CHEN, Q. XU and R. Z. YUAN, *Comp. Sci. Tech.* **61** (2001) 935.
7. D. Y. GODOVSKI, *Adv. Polym. Sci.*, **119** (1995) 79.
8. A. BANDYOPADHYAY, M. D. SARKAR and A. K. BHOWMICK, *J. Appl. Polym. Sci.* **95** (2005) 1418.
9. *Idem.*, *Rubber Chem. Technol.* **77** (2004) 830.
10. M. MAITY, S. SADHU and A. K. BHOWMICK, *J Polym Sci. Part B: Polym. Phy.* **42** (2004) 4489.
11. S. SADHU and A. K. BHOWMICK, *Adv. Engg. Mater*, **6** (2004) 738.
12. *Idem.*, *J. Polym Sci. Part B: Polym. Phy.* **42** (2004) 1573.
13. *Idem.*, *Rubber Chem. Technol.* **76** (2003) 860.
14. L. XILONG, S. ZHOU, L. WU, B. WANG and L. YANG, *Polymer* **45** (2001) 860.
15. B. K. COLTRAIN, C. J. T. LANDRY, J. M. O'REILLY, A. M. CHAMBERLAIN, G. A. RAKES, J. S. SEDITA, L. W. KELTS, M. R. LANDRY and V. K. LONG, *Chem. Mater.* **5** (1993) 1445.
16. C. C. SUN and J. E. MARK, *Polymer* **30** (1989) 104.
17. Z. AHMAD, M. I. SARWAR and J. E. MARK, *J. Mater. Chem.* **7** (1997) 259.
18. G. S. SUR and J. E. MARK, *Eur. Polym. J.* **21** (1985) 1051.
19. B. SMARSLY, G. GARNWEITNER, R. ASSINK and C. J. BRINKER, *Prog. Org. Coatings* **47** (2002) 393.
20. G. KICKELBICK, *Prog. Polym. Sci.* **28** (2003) 83.
21. Y. P. WANG, X. W. PEI, X. Y. HE and K. YUAN, *Euro. Polym. J.* **41** (2005) 1326.
22. C. L. JACKSON, B. J. BAUER, A. I. NAKATANI and J. D. BARNES, *Chem. Mater.* **8** (1996) 727.
23. P. HAJJI, L. DAVID, J. F. GERAND and G. VIGIER, *J. Polym. Sci. Part B: Polym. Phy.* **37** (1999) 3172.
24. R. TAMAKI and Y. J. CHUJO, *Mater. Chem.* **8** (1998) 1113.
25. G. SOCRATES, Infrared Characteristic Group Frequencies, John Wiley (New York 1980).
26. S. D. L. MARTINO and M. KELCHTERMANS, *J. Appl. Polym. Sci.* **56** (1995) 1781.
27. S. PATEL, A. BANDYOPADHYAY, V. VIJAYABASKAR, A. K. BHOWMICK, *Polymer* **46** (2005) 8079.
28. W. W. SIMONS "The Sadtler Guide to Carbon -13 NMR Spectra," Sadtler Research Laboratories, 1983.
29. A. K. BHOWMICK, Invited Lecture, International Workshop on Polymer Nanocomposites: Recent Developments and Applications, Melbourne, Australia, May 23–25, 2005.